THE JOURNAL OF PHYSICAL CHEMISTRY B

Article

pubs.acs.org/JPCB

Formation of Tubular Scrolls with Controlled Internal Cavity

Minwoo Han and Eunji Sim*

Department of Chemistry and Institute of Nano-Bio Molecular Assemblies, Yonsei University, 50 Yonsei-ro Seodaemun-gu, Seoul 120-749, Korea

ABSTRACT: In this work, we investigate internal cavity controlled tubular scroll formation through simple modification of tether coils that are grafted on the surface of a 2D polymer sheet. Dissipative particle dynamics simulations show that coarse-grained 2D sheets transform to various cylindrical structures including tubular and filled scrolls in the presence of broken volume and chemical symmetries of tether coils: volume (chemical) asymmetry arises when coils on one side have a different number of beads (solvent affinity) from those on the other side. It is clear from a phase diagram that the scroll formation is governed by the balance between hydrophobicity and entropy of coils. The density profiles show that a wide range of interior cavity diameter can be obtained by employing volume asymmetry on coils with weak chemical asymmetry. We provide crucial scientific insights in understanding the scroll formation through self-assembly of rod−coil molecules and suggest modification of the tether coil's properties as a practical and systematic method to form tubular scrolls with targeted internal cavity.

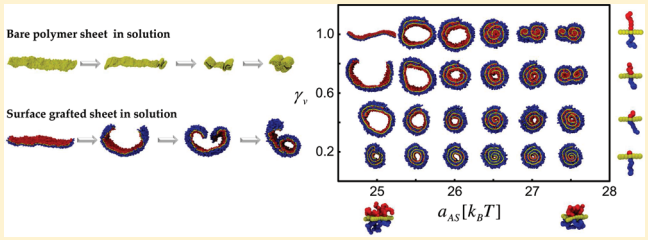

I. INTRODUCTION

For many years, nanosized tubular scrolls including carbon nanotubes have been studied experimentally[1−9] and theoretically.[10−12] In particular, the size of the internal cavity is one of the most interesting characteristics of tubular scrolls because the hollow interior enables medical and industrial encapsulation applications.[1−3] For instance, while adjusting the amount of delivered encapsulant is a simple matter of changing the number of dispensed scrolls, some properties such as the encapsulant time-release profile are expected to depend intimately upon scroll length and internal cavity diameter.[4,13] Internal cavity diameter also governs the particle mean deposition distance, and thus, regulation of the hollow interior is crucial for biomedical applications.[5,6,14]

Experimentally, tubular scrolls are formed in various ways: layered materials roll up in solutions and films[7,8,15] and structure-guiding templates such as coating pores[16] or core elimination of a core−shell nanowire are common.[17,18] In addition, self-assembled nano- and microtubules were reported in the presence of hydrogen bonding both in aqueous solutions[19] and in solid states.[20] It has been theoretically known that the anisotropy in two-dimensional (2D) sheets causes various curved phases including tubular scrolls.[10−12] Owing to the development of various simulation tools, formation of curved structures from an anisotropic 2D sheet has recently been illustrated: coarse-grained models combined with Brownian dynamics,[20] molecular dynamics,[21] and Monte Carlo simulation methods[11] have reproduced experimentally observed scroll formation phenomena. Furthermore, novel approaches to control tubular scroll dimension have also been reported in which the diameter of supramolecular tubular scrolls was successfully regulated by chemical modifications of molecular structures.[1,2] Despite extensive efforts on exploring the tubular scroll formation process, understanding of the relationship between the type of sheet anisotropy and the scroll morphology lacks and, thus, formation of well-defined tubular scrolls as well as control of its internal cavity still remain challenging.

Here we search for the main factors that govern the morphology of scrolls and suggest a systematic way to control its internal cavity and kinetics of scroll formation. Sheet properties are also important; for instance, the bonding constant strength of sheet beads, i.e., type and strength of aggregation force to form the sheet, plays an important role in determining the degree of sheet bending.[11] Therefore, the relationship between the degree of sheet bending and bond strength is needed for the cluster structure prediction and tubular scroll design. Motivated by the recent observation of reversible transformation of a surface grafted 2D polymer sheet to tubular scroll as a function of temperature,[7] we focus on the influence of tether coil properties on scroll formation. Alteration of tether coil properties of rod−coil amphiphiles is relatively simple yet effective in inducing various types and degrees of sheet anisotropy. Therefore, we seek the relationship between the size of the hollow interior and molecular/environmental properties to shed light on the manipulation of the internal cavity through modification of tether properties or solvent composition. Formation and application of nanotubules are performed often in the condensed phase in which environmental properties affect the self-assembly process significantly. The dissipative particle dynamics (DPD) method is reliable and accurate in describing environmental properties, such as the hydrodynamic effect.[22−28] Therefore, it is appropriate to use the DPD method to elucidate the scroll formation under the influence of the medium.

Received: November 2, 2011
Revised: December 29, 2011
Published: February 6, 2012

dx.doi.org/10.1021/jp2105083 | J. Phys. Chem. B 2012, 116, 1796−1801

This article is organized as follows: A brief description of DPD simulations and the coarse-grained model is presented in section II. In section III, transformation of a surface grafted polymer sheet is explored with respect to the anisotropy imposed on the sheet. Concluding remarks appear in section IV.

II. MODEL AND METHOD

Transformation of a 2D sheet in solutions is investigated using DPD simulations on a coarse-grained model. The model replaces a group of atoms with a single coarse-grained bead enabling highly efficient computation compared to all-atom molecular dynamics (MD) simulations by roughly 10^4–10^7 times.[26] Fundamentals of both algorithms are based on classical mechanics. In DPD methods, however, in addition to the conservative force ($\mathbf{F}_{ij}^{C}$), the total force on a particle i ($\mathbf{F}_i$) includes a dissipative force ($\mathbf{F}_{ij}^{D}$) and a random force ($\mathbf{F}_{ij}^{R}$) acting between ith and jth particles such that[29]

$$\mathbf{F}_i = \sum_{i \neq j} (\mathbf{F}_{ij}^{C} + \mathbf{F}_{ij}^{D} + \mathbf{F}_{ij}^{R}) \tag{1}$$

The functional forms of the force components between the ith particle at $\mathbf{r}_i$ with the velocity $\mathbf{v}_i$ and the jth particle at $\mathbf{r}_j$ with $\mathbf{v}_j$ are expressed as[26]

$$\mathbf{F}_{ij}^{C} = a_{ij}(1 - r_{ij}/r_c)\hat{r}_{ij} \tag{2}$$

$$\mathbf{F}_{ij}^{D} = -\gamma(1 - r_{ij}/r_c)^2(\hat{r}_{ij}\cdot(\mathbf{v}_i - \mathbf{v}_j))\hat{r}_{ij} \tag{3}$$

$$\mathbf{F}_{ij}^{R} = \sigma(1 - r_{ij}/r_c)\zeta_{ij}\Delta t^{-1/2}\hat{r}_{ij} \tag{4}$$

for $r_{ij} = |r_{ij}\hat{r}_{ij}| = |\mathbf{r}_i - \mathbf{r}_j| \leq r_c$. The forces are designed so that particles do not interact when they are farther apart than the cutoff distance, r_c, which is set as the unit length in simulations. Various parameters are used to control the interaction between DPD beads: a_{ij} represents the repulsion strength between particles i and j; the dissipation strength, $\gamma = 4.5$; and the random noise strength, $\sigma = 3.0$[30] to control the temperature as $\sigma^2 = 2\gamma k_B T$. Δt is the propagation time step, and ζ_{ij} is a Gaussian random number with zero mean and unit variance.[26]

Recent studies showed that laterally grafted rod–coil molecules produce various secondary cluster structures including columnar, lamellar, and tubular scroll phases.[7,20,31] Here we consider a self-assembly of laterally grafted rod amphiphiles consisting of double tether coils that are attached opposite to each other at the midpoint of the rod, as depicted in Scheme 1a. This kind of molecules is found to form a flat 2D sheet and to undergo transformation to a scroll as a function of temperature.[7] Therefore, we constructed a well-ordered 2D sheet as drawn in Scheme 1b as the initial structure for simulations and altered the tether coil properties to gain insights into the role of tether coils on scroll transformation. The coils are attached to the sheet in every seven rod beads to place adjacent coils as far as possible to ensure free volume to prevent overcrowding of tether coils. In Scheme 1a, the tether coils on one side are called **A**-coils (symbol **A**, red bead) and those on the other side are called **B**-coils (symbol **B**, blue beads), while **R** and **S** denote, respectively, a sheet formed by rod beads (yellow beads) and solvent beads throughout the article.

All sheet beads and coil beads within a single chain are bonded with harmonic springs: each of the bonded ith and jth beads are connected by $\mathbf{F}_{ij}^{S} = k(\bar{r} - r_{ij}/r_c)\hat{r}_{ij}$ with a force constant of k and an equilibrium distance $\bar{r}$ corresponding to bead types.

Scheme 1. (a) Coarse-Grained Model of a Laterally Grafted Rod–Coil Molecule and (b) Top View of the Initial Structure of Surface Grafted 2D Polymer Sheet Model[a]

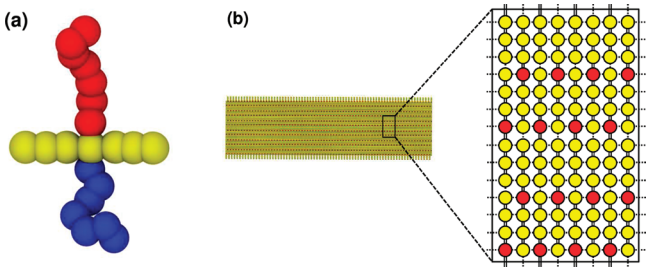

[a]The red beads in part b denote the coil tethered position. We assumed that upper and lower side tether coils are attached to the same rod bead. The dotted lines connecting beads denote inter-rod interaction by harmonic springs, while the double solid lines denote intra-rod harmonic bonding with angle constraint.

By assigning one bead per phenyl group, it is reasonable to assume $\bar{r}_{intra} = \bar{r}_{inter}$, since the diameter of a benzene (~3 Å) is close to the known π–π stacking distance (3–4 Å). Phenyl groups of the rod are covalently bonded, while molecular aggregation is driven by π–π stacking. In order to describe different types of chemical bonding and/or interaction, inter-rod interaction was modeled to be weaker than intrarod interaction. Although sheet beads are bound at short equilibrium distances, the weak inter-rod force constant along with a soft repulsive DPD potential allows sheet beads to be easily displaced and extended from their equilibrium distance. In order to model the rigidity of the rod, harmonic angle constraint is also applied in parallel to the rod direction along the short side of the sheet:[21] as schematically drawn in Scheme 1b, intrarod beads have angle constraints as well as harmonic bond springs. The rigidity of the rod is represented by $f_{ij}^{A} = k_{ang}(\theta - \bar{\theta})$ with an equilibrium angle $\bar{\theta}$. On the contrary, inter-rod bead interaction is defined only by harmonic springs.

The aspect ratio of the 2D sheet was chosen to be 2:7. A surface grafted 2D polymer sheet is placed inside a simulation box which is filled with single bead solvent molecules. The DPD potential parameters used for the models are listed in Table 1. Three initial structures were simulated under each condition. The total number of beads in the simulation box is 675 000 (number density of the system, $\rho = 3$) including solvent beads. All simulations were performed with the LAMMPS package[32] with the time step $\Delta t = 0.02\tau$, and the temperature was maintained at 0.3 in DPD reduced units.[26] VMD was used for visualization.[33]

III. RESULTS AND DISCUSSION

It has long been predicted that 2D anisotropic sheets with a long-range orientational order form a scroll phase.[10–12] Existence of angular constraint along the rod axis in Scheme 1b leads to the formation of in-plane anisotropic sheets. Thus, the 2D sheet collapses to a crumpled cylinder along the rod orientation axis, as shown in Figure 1a. On the other hand, by attaching surface tethers onto the identical polymer sheet, strikingly different curved structures resulted as in Figure 1b. In order to explore the role of surface tethers as well as the influence of the type and degree of surface anisotropy, we implemented broken tether symmetry in two aspects: volume and chemical asymmetry. The volume asymmetry arises when coils on one side have a different number of beads from those

dx.doi.org/10.1021/jp2105083 | J. Phys. Chem. B 2012, 116, 1796–1801

Table 1. DPD Potential Parameters: Repulsion Parameter, $a_{\alpha\beta}$, Force Constant, k, and Equilibrium Bond Distance and Angle, $\bar{r}$ and $\bar{\theta}$[a]

tether coil						sheet						
$a_{\alpha\alpha}$ α = A, B, R, S	a_{AS}	a_{BS}	a_{AB}	k_{coil}	$\bar{r}_{coil}$	$a_{R\beta}$ β = A,B,S	k_{intra}	k_{inter}	$\bar{r}_{intra}$	$\bar{r}_{inter}$	k_{ang}	$\bar{\theta}_{ang\ (deg)}$
25	25−28	25	20	25	0.5	30	100	50	0.5	0.5	40	180

[a]In subscripts, A, B, R, and S represent, respectively, **A**-coil, **B**-coil, sheet, and solvent beads, intra (inter) denotes intra-rod (inter-rod) interaction, and ang denotes angular constraint. $a_{\alpha\beta}$ is in k_BT units.

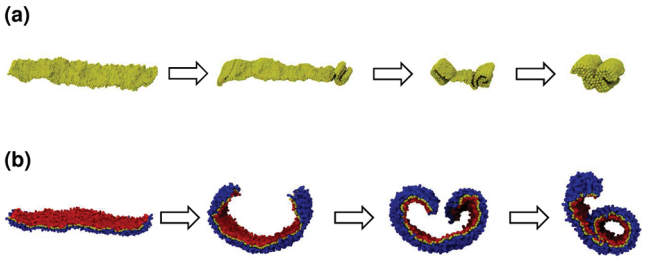

Figure 1. (a) Crumpled cylinder phase formed from a 2D polymer sheet and (b) curved sheet and scroll phase from a surface grafted 2D polymer sheet. For comparison, the same polymer sheet model was used for parts a and b.

on the other side, while the chemical asymmetry refers to the coil−solvent affinity difference. The phase diagram in Figure 2

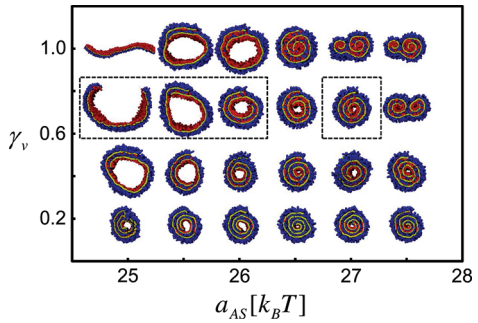

Figure 2. Phase diagram of the surface grafted 2D polymer sheet. Instead of the full picture, cross sections of curved structures are shown to demonstrate local curvature and to emphasize the presence of the internal cavity. $\gamma_V = N_A/N_B$ represents the volume asymmetry between **A**-coil (upper) and **B**-coil (lower) beads, and a_{AS} describes the solvent affinity of **A**-coils. While the **B**-coil consists of seven beads ($N_A = 7$) for all models, the number of beads in the **A**-coil, N_A, varies from 1 to 7. Cross sections are drawn to their relative sizes except for the fluctuating 2D sheet and the curved sheet, which are shrunken to fit.

shows the formation of curved sheets, tubular and filled scrolls as a function of tether coil volume ratio, γ_V, and **A**-coil−solvent repulsion strength, a_{AS}. Because we assumed an equal volume for a bead regardless of the type, the tether coil volume ratio is equal to the bead number ratio, i.e., $\gamma_V = N_A/N_B$, where the **A**(**B**)-coil consists of N_A (N_B) beads. The volume asymmetry is applied with $1 \le N_A \le 7$ while maintaining $N_B = 7$: γ_V ranges from 0.13 (severe volume asymmetry, 1−7[$N_A = 1$ and $N_B = 7$] models) to 1.0 (no volume asymmetry, 7−7 models). On the contrary, for the chemical asymmetry, **A**-coil−solvent interaction is altered from theta to bad solvent interaction ($25k_BT \le a_{AS} \le 27.5k_BT$), while **B**-coil remains to be at its theta solvent condition ($a_{BS} = 25k_BT$). Snapshots taken at 6×10^6 steps of the simulation appear in Figure 2. Since the 2D sheet model is identical for all simulations, various morphologies of scroll structure arise due to the asymmetric properties of surface tethers which are grafted on the upper and lower side of the sheet. Note that the DPD potential provided repulsive interactions between beads so that curve formation was driven purely by the anisotropy of the surface grafted sheet without artificial pulling or attraction between coil beads. In ref 7, rod amphiphiles are laterally grafted with double tether coils that are mainly composed of ether moieties. Molecular interaction between nonbonded ethers from a chain and that from separate chains are modeled indistinguishable. For the sake of computational efficiency, relatively less repulsive force was applied for heterogeneous coil interactions. The magnitude of a_{AB} has no noticeable influence on the results presented here, since **A**- and **B**-coils interact with each other when the two opposite ends of the polymer sheet are already close to form scrolls.

The structures on the far left of Figure 2 represent the influence of tether coil volume symmetry. We assumed that all coils consist of a single type of chemical species by setting the solvent−coil interaction to be equivalent as $a_{AS} = a_{BS} = 25k_BT$. Only the number of coil beads in a chain is different depending on the coil type. The curvature of the grafted sheet depends on the degree of volume symmetry: The 7−7 model ($\gamma_V = 1.0$) shows only thermal fluctuation for the entire simulation time, and the 5−7 model ($\gamma_V = 0.71$) forms a slightly curved sheet. As the degree of volume symmetry decreases, the sheet curvature becomes larger and eventually tubular scrolls were formed for the 3−7 ($\gamma_V = 0.43$) and 1−7 ($\gamma_V = 0.14$) models. Since the two short ends should make contact to form a scroll, formation of tubular scrolls is also relevant to the sheet aspect ratio. Note that sheet models with a 2:7 aspect ratio were used for this work. With the use of a longer sheet, the curved sheet in Figure 2 may become a tubular scroll with a large internal cavity.

The structures at the top of Figure 2 illustrate the influence of chemical symmetry on 7−7 models. In the presence of even a weak coil−solvent affinity difference between upper and lower surface tethers, a fluctuating sheet rolls into a tubular scroll. Due to hydrophobicity, **A**-coils repel solvent beads and aggregate among themselves which, in turn, leads to curved structures. Hydrophobic **A**-coils prefer closing the hollow interior to avoid unstable solvent contact. Even so, there is apparently a large internal cavity in the center of tubular scrolls of $a_{AS} = 25.5k_BT$ and $26k_BT$ models owing to entropic repulsion between **A**-coil beads.

Overall, the lower the degree of tether coil symmetry, the higher the local curvature regardless of the asymmetry type, which is reflected in the magnitude of curve formation rate. However, structural change induced by the volume asymmetry is smaller than what is caused by the chemical asymmetry: in the absence of chemical asymmetry, severe volume asymmetry ($\gamma_V < 0.5$) is required to form a scroll from a flat sheet. On the contrary, little change in solvent affinity affects the sheet curvature significantly, as seen for $a_{AS} = 25.5k_BT$ models. Therefore, the combination of volume and chemical asymmetry produces tubular scrolls with various sizes of internal cavity, as

dx.doi.org/10.1021/jp2105083 | J. Phys. Chem. B 2012, 116, 1796−1801

illustrated in the phase diagram. The three double scroll structures in the upper right corner of Figure 2 are local minimum structures whose free energy is very close to the global minimum. Double scroll structures are initial state dependent and can be obtained when the scroll formation rate is rather high so that both ends of the polymer sheet roll fast and two large rolls meet in the middle. Although they are kinetically trapped at the local free energy minima, they may transform to single scrolls for which the free energy is indeed minimal.

Previous theoretical and experimental works have predicted a cylindrical or tubular phase of a polymer sheet.[7,20,34] However, details on the formation kinetics are insufficient. In order to demonstrate the formation kinetics, four representative curved structures from Figure 2 (dotted box) are selected (a curved sheet, single- and multiwalled tubular scrolls, and a filled scroll) and their cross sections and side views are shown in Figure 3a. Figure 3b presents the

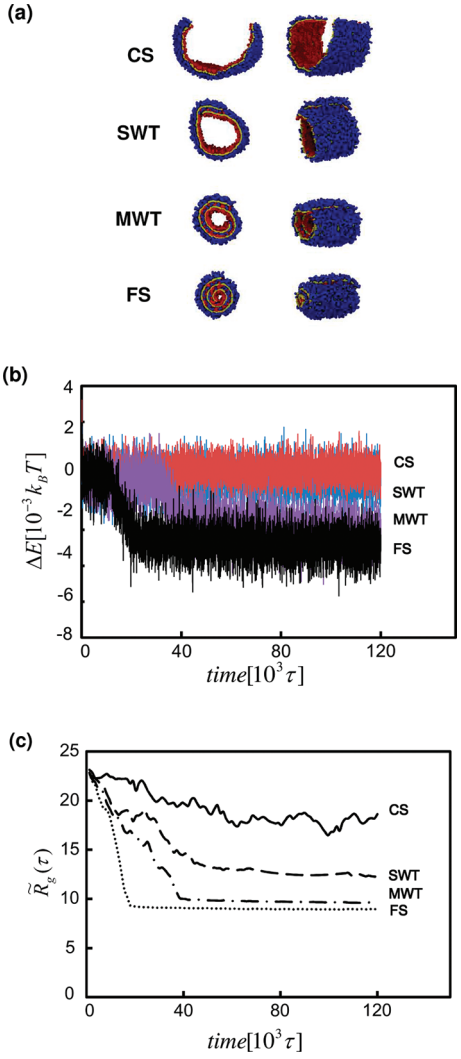

Figure 3. (a) Selected four structures noted in the dotted box of Figure 2 and their energy profile in part b and radius of gyration in part c. CS stands for a curved sheet, SWT for a single-walled tubular scroll, MWT for a multiwalled tubular scroll, and FS for a filled scroll. All models are from the 5−7 models (γ_V = 0.73) with, respectively, a_{AS} = 25k_BT (CS), 25.5k_BT (SWT), 26k_BT (MWT), and 27k_BT (FS).

corresponding total energy change in the course of curve formation and scrolling. It is obvious that the energy becomes lower as the sheet forms a structure with higher curvature and, thus, a filled scroll is the most stable. Instead of absolute total energy, we compare the energy difference from the corresponding initial structure, since each model has different potential parameters.

The kinetics of a structural change is analyzed quantitatively by means of the radius of gyration, $\tilde{R}_g(t)$, which is evaluated as

$$\tilde{R}_g(t) = \sqrt{\bar{R}_{xx}^{\,2}(t) + \bar{R}_{yy}^{\,2}(t) + \bar{R}_{zz}^{\,2}(t)} \quad (5)$$

$\bar{R}_{\alpha\alpha}(t)$ (α = x,y,z) denotes the time evolution of the three principal radii of gyration obtained from the radius of gyration tensor. Its elements are

$$R_{\gamma\delta} = \frac{1}{N_{sheet}} \sum_{i=1}^{N_{sheet}} (\gamma_i - \gamma_{CM})(\delta_i - \delta_{CM}) \quad (6)$$

where γ_i and δ_i are the x, y, and z coordinate of ith bead of the sheet. γ_{CM} and δ_{CM} are those of the center of mass of a sheet consisting of N_{sheet} beads. The magnitude of $\tilde{R}_g(t)$ effectively demonstrates polymer sheet curvature at a given time: large $\tilde{R}_g(t)$ means a slightly curved sheet, while small $\tilde{R}_g(t)$ describes a large curved or scrolled structure. Figure 3c presents the time evolution of $\tilde{R}_g(t)$ of the four previously selected models. Clearly, large chemical asymmetry results in a structure of high local curvature: the curved sheet at a_{AS} = 25k_BT, the single-walled tubular scroll at 25.5k_BT, the multiwalled tubular scroll at 26k_BT, and the filled scroll at 27k_BT. Initially large $\tilde{R}_g(t)$ of a flat sheet decreases with time as it forms a curved structure. In particular, $\tilde{R}_g(t)$ of the model that produces a scroll decreases drastically. The magnitude of the curve formation rate, i.e., the initial slope of $\tilde{R}_g(t)$, has strong correlation with the morphology of the final structure: a higher rate would tend to correlate with a stable structure of a smaller internal cavity. Figure 4 shows the dependence of curve formation rate on the

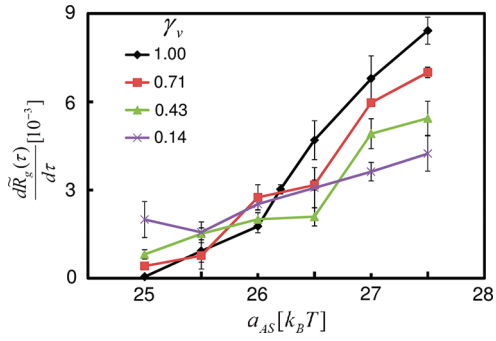

Figure 4. Curve formation rate with respect to the solvent affinity of **A**-coils, a_{AS}. For each data point, three uncorrelated initial structures were simulated and error bars are employed to demonstrate the sensitivity of initial structures.

sheet anisotropy owing to the broken tether coil symmetries. At a_{AS} = 25k_BT(chemically symmetric tethers), the rate is higher for smaller γ_V, indicating that entropic repulsion between coil beads governs the curve formation process. On the other hand, at a_{AS} = 27.5k_BT (severe chemical asymmetry models), the magnitude of the curve formation rate shows an exactly opposite sequence. The rates at a_{AS} > 25k_BT resulted from the competition between entropic repulsion and solvent affinity of **A**-coils. Since the hydrophobicity of the **A**-coil increases with the number of beads, the effect of the solvent affinity difference is more prominent for the 7−7 models than the others. This is also obvious from the fact that the overall change is greater for larger γ_V models as a_{AS} varies from 25k_BT to 27.5k_BT.

dx.doi.org/10.1021/jp2105083 | J. Phys. Chem. B 2012, 116, 1796−1801

For all scrolls, a rapid decrease of $\tilde{R}_g(t)$ continues until two short ends of the sheet make contact with each other. Subsequently, affinity or relative repulsion between **A**- and **B**-coils stabilizes the scroll structures. As can be seen in Figure 3c, the hollow interior closing rate is very low. In other words, once a tubular scroll is formed, the structure is stable for a fairly long time of simulation even in the presence of unstable hydrophobic coil−solvent contact in the hollow interior.

In order to control the tubular scroll, we have explored the relationship between the internal cavity and the sheet anisotropy. Figure 5 presents density profiles of the three representative scroll

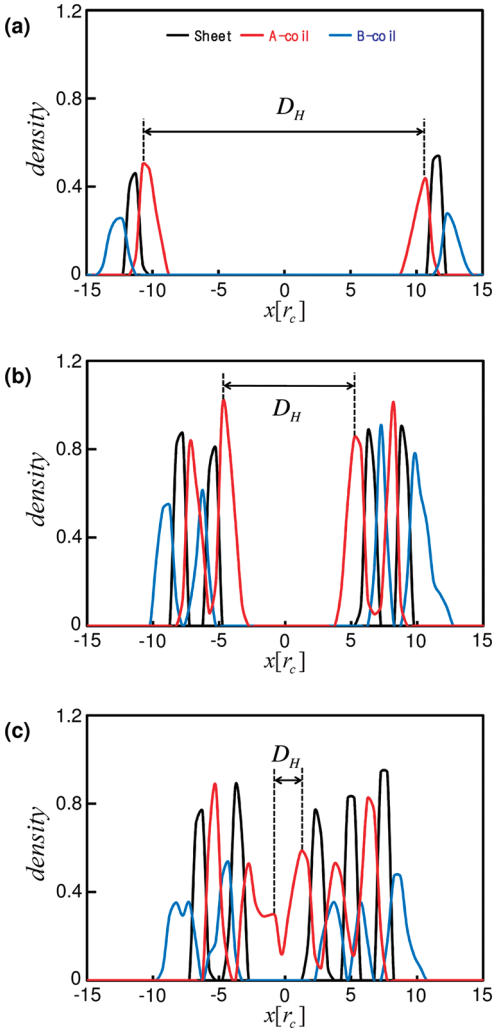

Figure 5. Density profiles of the three selected scroll structures inside the dotted box of Figure 2. The solvent affinity of **A**-coils, a_{AS}, is (a) $25.5k_BT$, (b) $26k_BT$, and (c) $27k_BT$. Each line represents different types of beads: sheet (black line), **A**-coil (red line), and **B**-coil (blue line). Solvent beads are omitted for clarity.

structures of Figure 3a. For clarity, solvent beads are omitted from visualization. For the density profile evaluation, the scroll is rotated to be perpendicular to a rectangular box: the average unit vector of the scroll is calculated from the rods' unit vectors and then a rectangular box is chosen such that its center coincides with the center of mass of the scroll while the long axis is perpendicular to the scroll's average unit vector. The average density distribution of beads is evaluated along the cross section of the scroll. From the density profiles, the diameter of the internal cavity is estimated, which is defined as the distance between opposite red peaks (most probable position of **A**-coil beads) that are closest to the center of the scroll. In Figure 6, the

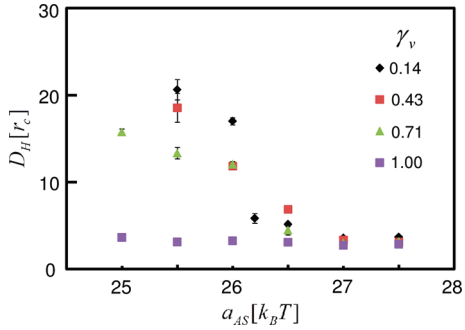

Figure 6. Relationship between the internal cavity diameter, D_H, of a scroll and the solvent affinity of **A**-coils, a_{AS}. For each data point, three uncorrelated initial structures were simulated and error bars are employed to demonstrate the sensitivity of initial structures. In some cases, error bars are smaller than markers.

internal cavity diameter obviously decreases as the **A**-coil−solvent repulsion increases. Except for the 1−7 (γ_V = 0.14) models, a wide range of the internal cavity diameter was observed. With hydrophilic or weakly hydrophobic **A**-coils, single-walled tubular scrolls with a large hollow interior were formed. In fact, the longer the hydrophobic coil, the larger the internal cavity. In contrast, with strongly hydrophobic **A**-coils, scrolled structures are formed, since the interaction between **A**-coil−solvent beads overcomes entropic repulsion of the **A**-coil. For intermediate models, however, entropic repulsion and hydrophobicity of the **A**-coil are competitive to each other and multiwalled tubular scrolls are formed. The internal cavity diameter is a direct indicator of the relative strength of the entropic repulsion and the hydrophobicity of **A**-coils. Severe volume asymmetry in 1−7 models results in scrolls with small or negligible hollow interior depending on the degree of chemical asymmetry because the **A**-coil is too short to provide entropic repulsion that is required to preserve the internal cavity.

We emphasize that the internal cavity diameter can be widely varied when one side of the surface is grafted with weakly hydrophobic coils. This implies that tubular scrolls with targeted internal cavity can be obtained by applying coil volume asymmetry on a surface grafted polymer sheet. The results in this article agree excellently with previous experiments and provide an explanation of the observations: rod−coil molecules formed spontaneous curvature as a function of temperature,[7] and the dimension of biomimetic tubular scrolls was regulated through chemical modifications of molecular structures.[1,2] The combination of appropriate volume and chemical coil asymmetries may provide an alternative way to manipulate the hollow interior of tubular scrolls in a feasible way.

IV. CONCLUDING REMARKS

There are several factors that cause anisotropy on a 2D polymer sheet and lead to the formation of scrolls, mainly, volume and chemical asymmetry of tether coils and sheet stiffness. In this work, we successfully transformed fluctuating 2D sheets to various cylindrical structures through simple modification of tether coil properties. More importantly, we showed that the internal cavity of tubular scrolls can also be delicately controlled. The phase diagram of a surface grafted 2D polymer sheet with respect to coil−solvent affinity and tether coil volume

dx.doi.org/10.1021/jp2105083 | J. Phys. Chem. B 2012, 116, 1796−1801

asymmetry indeed illustrated that tether coil modification would allow a controllable way to scroll formation with variable internal cavity. When the two surfaces of a polymer sheet are grafted with coils whose chemical properties are weakly asymmetric, the balance between hydrophobicity and entropy of tether coils determines the hollow interior. Hydrophobic coils minimize solvent contact so that filled scrolls are preferred while tubular scrolls are formed in the presence of volume asymmetric surface tethers. The scroll formation rate is also affected by the balance of surface tension between tether coils on either side of the sheet surface. When the two opposite ends of the sheet make contact, the rate of internal cavity closure becomes rather low and almost no change in the scroll structures was observed for a fairly long simulation time. The findings in this article provide crucial scientific insights in understanding the scroll formation through self-assembly of rod−coil molecules. We, thus, envision that the modification of the tether coil's volume and chemical properties would lead to a practical and systematic method to form tubular scrolls with targeted internal cavity.

AUTHOR INFORMATION

Corresponding Author

*E-mail: esim@yonsei.ac.kr. Fax: +82-2-364-7050.

ACKNOWLEDGMENTS

This work was supported by the global research network grant (NRF-2010-220-C00017) and the basic science grants (2011-0002832 and 2011-0003690) funded by the national research foundation (NRF). M.H. also appreciates the fellowship of the BK21 program from MOEHRD. E.S. also appreciates Myongsoo Lee for insightful and valuable discussions.

REFERENCES

(1) Shimizu, T. *J. Polym. Sci., Part A: Polym. Chem.* **2006**, *44*, 5137−5152.
(2) Tarabout, C.; Roux, S.; Gobeaux, F.; Fay, N.; Pouget, E.; Meriadec, C.; Ligeti, M.; Thomas, D.; IJsselstijn, M.; Besselievre, F.; Buisson, D.-A.; Verbavatz, J.-M.; Petitjean, M.; Valéry, C.; Perrin, L.; Rousseau, B.; Artzner, F.; Paternostre, M.; Cintrat, J.-C. *Proc. Natl Acad. Sci. U.S.A.* **2011**, *108*, 7679−7684.
(3) Wang, B.; Poa, C. H. P.; Wei, L.; Li, L.-J.; Yang, Y.; Chen, Y. *J. Am. Chem. Soc.* **2007**, *129*, 9014−9019.
(4) Jin fan, H.; Knez, M.; Scholz, R.; Nielsch, K.; Pippel, E.; Hesse, D.; Zacharias, M.; Gosele, U. *Nat. Mater.* **2006**, *5*, 627−631.
(5) Son, S. J.; Bai, X.; Nan, A.; Ghandehari, H.; Lee, S. B. *J. Controlled Release* **2006**, *114*, 143−152.
(6) Leila, Z. *J. Controlled Release* **2002**, *81*, 7−23.
(7) Lee, E.; Kim, J.-K.; Lee, M. *Angew. Chem., Int. Ed.* **2009**, *121*, 3711−3714.
(8) Li, Y. D.; Li, X. L.; He, R. R.; Zhu, J.; Deng, Z. X. *J. Am. Chem. Soc.* **2002**, *124*, 1411−1416.
(9) Fan, H. J.; Gösele, U.; Zacharias, M. *Small* **2007**, *3*, 1660−1671.
(10) Radzihovsky, L.; Toner, J. *Phys. Rev. Lett.* **1995**, *75*, 4752−4755.
(11) Bowick, M.; Falcioni, M.; Thorleifsson, G. *Phys. Rev. E* **1997**, *79*, 885−888.
(12) Stenull, O. *Phys. Rev. E* **2008**, *78*, 031704.
(13) Mishra, B. K.; Thomas, B. N. *J. Am. Chem. Soc.* **2002**, *124*, 6866−6871.
(14) Johnson, D. L.; Esmen, N. A.; Carlson, K. D.; Pearce, T. A.; Thomas, B. N. *J. Aerosol Sci.* **2000**, *31*, 181−188.
(15) Schmidt, O. G.; Eberl, K. *Nature* **2001**, *410*, 168−168.
(16) Steinhart, M.; Wendorff, J. H.; Greiner, A.; Wehrspohn, R. B.; Nielsch, K.; Schilling, J.; Choi, J.; Gösele, U. *Science* **2002**, *296*, 1997.
(17) Liu, Z.; Zhang, D.; Han, S.; Li, C.; Lei, B.; Lu, W.; Fang, J.; Zhou, C. *J. Am. Chem. Soc.* **2004**, *127*, 6−7.
(18) Yan, Y.; Lin, Y.; Qiao, Y.; Huang, J. *Soft Matter* **2011**, *7*, 6385−6398.
(19) Jiang, L.; Peng, Y.; Yan, Y.; Deng, M.; Wang, Y.; Huang, J. *Soft Matter* **2010**, *6*, 1731−1736.
(20) Hong, D.-J.; Lee, E.; Jeong, H.; Lee, J.-k.; Zin, W.-C.; Nguyen, T. D.; Glotzer, S. C.; Lee, M. *Angew. Chem., Int. Ed.* **2009**, *48*, 1664−1668.
(21) Knauert, S. T.; Douglas, J. F.; Starr, F. W. *Macromolecules* **2010**, *43*, 3438−3445.
(22) Groot, R. D.; Rabone, K. L. *Biophys. J.* **2001**, *81*, 725−736.
(23) He, L.; Zhang, L.; Ye, Y.; Liang, H. *J. Phys. Chem. B* **2010**, *114*, 7189−7200.
(24) Stevens, M. J.; Hoh, J. H.; Woolf, T. B. *Phys. Rev. Lett.* **2003**, *91*, 188102.
(25) Yang, K.; Ma, Y.-Q. *Nat. Nanotechnol.* **2010**, *5*, 579−583.
(26) Frenkel, D.; Smit, B. *Understanding Molecular Simulation*; Academic Press: San Diego, CA, 2002.
(27) Han, M.; Hong, M.; Sim, E. *J. Chem. Phys.* **2011**, *134*, 204901.
(28) Shillcock, J. C.; Lipowsky, R. *Nat. Mater.* **2005**, *4*, 225−228.
(29) Español, P.; Warren, P. *Europhys. Lett.* **1995**, *30*, 191.
(30) Groot, R. D.; Warren, P. B. *J. Chem. Phys.* **1997**, *107*, 4423−4435.
(31) Hong, D.-J.; Lee, E.; Lee, J.-K.; Zin, W.-C.; Han, M.; Sim, E.; Lee, M. *J. Am. Chem. Soc.* **2008**, *130*, 14448−14449.
(32) http://lammps.sandia.gov.
(33) Humphrey, W.; Dalke, A.; Schulten, K. *J. Mol. Graphics* **1996**, *14*, 33−38.
(34) Jiang, L.; Peng, Y.; Yan, Y.; Huang, J. *Soft Matter* **2011**, *7*, 1726−1731.